J Porous Mater (2015) 22:1511–1518
DOI 10.1007/s10934-015-0033-7

Synthesis, luminescent and drug-release properties of SiO_2@Y_2O_3:Eu hollow mesoporous microspheres

Hongfang Jiu[1] · Wanbao Jia[1] · Lixin Zhang[2] · Changshui Huang[1] · Hongqian Jiao[1] · Jianxia Chang[1]

Published online: 19 July 2015

Abstract SiO_2@Y_2O_3:Eu hollow mesoporous microspheres were prepared by coating luminescent Y_2O_3:Eu^{3+} particles onto uniform silica spheres using melamine formaldehyde microspheres as sacrificial templates. Various approaches including X-ray diffraction, scanning electron microscopy, transmission electron microscopy, Fourier transform infrared, thermogravimetric and differential thermal analysis, photoluminescence spectroscopy and N_2 adsorption/desorption were used to characterize the samples. The results indicate that Y_2O_3:Eu^{3+} particles have been coated onto the hollow silica spheres with 300 nm thickness shell, and the composite microspheres exhibit mesoporous characteristics and have spherical morphology. Upon ultraviolet excitation, the composite shows the characteristic $^5D_0$–$^7F_{1-4}$ red emission lines of Eu^{3+} even after loading of the model drug. In addition, drug release tests suggest that the composite has a controlled drug release property with ibuprofen as the model drug.

Keywords Y_2O_3:Eu^{3+} · Silica · Hollow · Drug release · Luminescence · Mesoporous

✉ Hongfang Jiu
hfjiu@126.com

[1] College of Science, North University of China, Taiyuan 030051, People's Republic of China

[2] Chemical Engineering and Environment Institute, North University of China, Taiyuan 030051, People's Republic of China

1 Introduction

In recent years, hollow-structured mesoporous spheres with photoluminescence (PL) properties aroused much attention because they have been extensively used as the most promising functional material in various biological fields [1–4]. In the fields of drug storage and delivery, hollow structured materials have gained special attention because they simultaneously have large voids and mesoporous shells [5–7]. The large voids make it possible to store more drug molecules than conventional materials. Also, the mesoporous shells can provide accessible channels for drug molecule diffusion and mass transfer. On the other hand, they can control the permeability of the shells for matter exchange between the outer environment and voids. Notably, fluorescence functionalized mesoporous silica drug delivery vehicle can be fabricated by the combination of mesoporous silica structure with fluorescent materials, and have attracted special interest because of their photoluminescence. Rare earth (RE) based materials exhibit good luminescent properties, chemical/photochemical inertness, and low toxicity, which seem to be excellent candidates for organic dyes and quantum dots [8–14]. Recently, many efforts have been devoted to preparing a series of muitifunctional composite using silica species as host materials and rare earth as luminescence material for drug storage and controlled release because of their non-toxic nature, high stability and good biocompatibility [7, 15–17]. Yang reported the fabrication, characterization of spherical $CaWO_4$:Ln @MCM-41(Ln = Eu^{3+}, Dy^{3+}, Sm^{3+}, Er^{3+}) composites and their applications as drug release systems [15]. Yang also demonstrated a magnetic, luminescent and mesoporous core–shell structured composite material (Fe_3O_4@nSiO_2@mSiO_2@YVO_4:Eu^{3+} composite microspheres) as drug carrier [16]. Gai showed

the synthesis, characterization, and application in controlled drug release of monodisperse core–shell-structured Fe_3O_4@nSiO_2@mSiO_2@$NaYF_4$:Yb^{3+}, Er^{3+}/Tm^{3+} nanocomposites [17]. Yang et al. [7] have reported that a novel bifunctional (fluorescent, mesoporous) hollow sphere for drug delivery vehicle was prepared by coating luminescent YBO_3:Eu^{3+} nanoparticles onto uniform hollow mesoporous silica spheres (HMSs).

Currently, synthetic strategies for the fabrication of porous/hollow structures mostly by well-established approaches involve the utilization of various removable templates, including soft ones such as surfactants, emulsion droplets, micelles, vesicles, ionic solvents and gas bubbles, and hard ones such as polymers, silica, carbon, metal oxides [18–24]. Because the melamine formaldehyde resin is very cheap, hollow spherical phosphors would achieve a reduction in the amount of expensive rare earth materials, and thus lower the cost of the rare earth luminescent materials. Recently, the melamine formaldehyde resin (MF) colloidal particles which act as a template have been steadily employed to fabricate hollow particles or hollow capsules [25–30]. Morever, yttrium oxide (Y_2O_3) is a promising host matrix for luminescence due to its good chemical durability, thermal stability, and low phonon energy. Cho et al. [31] showed the photoluminescence imaging of SiO_2@Y_2O_3:Eu(III) and SiO_2@Y_2O_3:Tb(III) core–shell nanostructures. However, to our knowledge, little attention has been paid to the preparation of hollow mesoporous composite microsphere (SiO_2@Y_2O_3) for drug storage and delivery by using MF colloidal particles as templates.

In this study, we developed a straight forward route to produce SiO_2 capsule coated Y_2O_3:Eu^{3+} (SiO_2@Y_2O_3:-Eu^{3+}) hollow composites with large hollow interiors using melamine formaldehyde (MF) microspheres as sacrificial templates. During the process, MF@SiO_2@$Y(OH)CO_3$:-Eu^{3+} were build as an core–shell composites precursor and subsequent removal of the core template and at the same time form the rare earth fluorescent materials by calcination. And ibuprofen (IBU) was picked as a model drug to illustrate the release properties of this functional composite.

2 Experimental sections

2.1 Chemicals and materials

Formaldehyde (37 %), melamine, polyvinyl alcohol (PVA), acetic acid, ammonia aqueous (28 wt%), Tetraethyl orthosilicate(TEOS, purity 99.8 %), hydrochloric acid (HCl, 37 %), absolute ethanol, cetyltrimethyammonium bromide (CTAB), $Y(NO_3)_3{\cdot}6H_2O$ (≥99.0 %, A. R.), and Eu_2O_3 (99.99 %), $CO(NH_2)_2$(urea), nitric acid (65 %), were obtained from Beijing Chemical Reagent Company. All chemicals were of analytical grade and were used as received without further purification. Deionized water was used for all experiments.

2.2 Synthesis of monodisperse MF microspheres

Monodisperse MF colloidal microspheres were prepared according to the literature with a modification [32]. Firstly, a solution of formaldehyde (5.3 mL, 37 %) was mixed with melamine (2.8 g) under stirring at 60 °C for 20 min to obtain a clear precursor solution. When the resulting precursor solution was cooled down to 35 °C, then poured it into 90 mL PVA solution (0.4 wt%), obtaining a mixture. Consequently, acetic acid was introduced into the mixture until the pH value was adjusted to 4.5 and the solution was then kept at a stirring condition at 65 °C for 30 min to obtain MF colloidal particles. White MF spheres were collected by centrifugation, washed three times with water and ethanol, and finally dried in air at 60 °C.

2.3 Synthesis of monodisperse MF@SiO_2 colloidal microspheres

Monodisperse MF@SiO_2 colloidal microspheres were prepared according to the literature with a modification [32]. In a typical preparation, as-prepared MF microsphere (0.2 g) was added and well dispersed into absolute alcohol (100 mL) with the assistance of ultrasound irradiation for 15 min. Then the MF alcohol suspension was transferred into a round-bottomed flask, a solution containing CTAB (0.05 g), aqueous NH_4OH (1 mL) and water (1 mL) was added into the above suspension at room temperature within 20 min under magnetic stirring. Subsequently, A TEOS alcohol solution (15 mL, 1 vol%) was added into the above mixture with a constant flow pump, after that the reaction process was allowed to sustain for 5 h at room temperature under continuous stirring. The core–shell composite spheres were separated from the suspension by centrifugation and washed three times with distilled water and ethanol. The solid was dispersed into an appropriate volume of deionized water and cooled to freeze; white powder, denoted as MF@SiO_2, was then obtained after a 24 h freeze-drying process and was preserved for subsequent experiments.

2.4 Synthesis of SiO_2@Y_2O_3:Eu^{3+} hollow mesoporous microspheres

In a typical synthesis of SiO_2@Y_2O_3:Eu^{3+} hollow mesoporous microspheres, 0.38 mmol of $Y(NO_3)_3{\cdot}6H_2O$ and 0.02 mmol of $Eu(NO_3)_3{\cdot}6H_2O$ were added to 200 mL of

distilled water. Then 1.0 g of urea was dissolved in the solution by vigorous stirring to form a clear solution. Subsequently, the MF@SiO_2 microspheres (1.0 g) were added and well dispersed into the above solution with the assistance of ultrasonication for 5 min. Finally, the mixture was transferred into a round-bottom flask and heated at 85 °C for 3 h with vigorous stirring. The precursor was collected by centrifugation and washed by deionized water and ethanol several times and dried at 60 °C in air. The final Y_2O_3:Eu^{3+}(5 mol%) hollow microspheres were obtained through a heat-treatment at 800 °C for 2 h in air with a heating rate of 2 °C min^{-1}.

2.5 Preparation of drug storage/delivery system

Typically, IBU was loaded to the sample as follows: 0.5 g of SiO_2@Y_2O_3:Eu^{3+} hollow microspheres were mixed with 0.2 g of IBU dispersed into 50 mL hexane solution. The mixture was allowed to stand at room temperature for 24 h, and the loaded materials were denoted as SiO_2@-Y_2O_3-IBU and rinsed three times with hexane and then dried under vacuum at 30 °C.

In vitro release profiles of IBU were evaluated by the dialysis method [33]. First, a dialysis bag (cut-off molecular weight 3000 Da) was filled with a SiO_2@Y_2O_3:Eu^{3+}-IBU buffer solution (5 mL, 20.0 mg mL^{-1}) and soaked in buffer solution(0.05 M, 45 mL) of pH 7.4 at 37 ± 1 °C in a water bath with gentle shaking under dark conditions. The released IBU outside of the dialysis bag was sampled at a predetermined time and measured by UV–Vis absorption at 263 nm and immediately replaced with an equal volume of fresh PBS.

2.6 Characterization

Powder X-ray diffraction (XRD) patterns were recorded on a TD-300 X-ray diffractometer with Cu KR radiation (40 kV,40 mA), transmission electron microscopy experiments (TEM) images were recorded on a Japan JEOL JEM-1400 microscope and scanning electronic microscope (SEM) image were recorded on an S-4800 electron microscope (Hitachi, Japan) operated at 200 kV. The photoluminescence (PL) spectra were recorded on a Edinburgh-FSP920 steady state and phosphorescence lifetime spectrometer with a Xe lamp at room temperature. Fourier transform infrared (FTIR) spectra were recorded on a SHIMAZU FTIR-8400 spectrometer with a potassium bromide (KBr) pellet technique. Thermogravimetric–differential thermoanalysis (TG–DTA) properties were recorded by China ZCT-2000 thermo-gravimetric analysis at a heating rate of 10 °C min^{-1}. Nitrogen adsorption desorption analysis was performed with a Micromeritics ASAP2020 (M + C) apparatus, and the specific surface area was determined by the Brunauer–Emmett–Teller (BET) method. The UV–Vis absorption spectral data were measured using a UV-2500 spectrophotometer.

3 Results and discussion

3.1 Phase, formation, morphology and structure of as-prepared samples

The crystallinity and the phase purity of the samples were examined by XRD. Figure 1 shows the XRD patterns of as-prepared precursor MF@SiO_2@$Y(OH)CO_3$:Eu^{3+} (a), and SiO_2@Y_2O_3:Eu^{3+} calcined at 800 °C (b). In Fig. 1a no obvious diffraction peak is observed, which implies that precursor without calcination belongs to the amorphous phase. The component of the amorphous precursor has been confirmed to be MF@SiO_2@$Y(OH)CO_3$:Eu^{3+} [34, 35]. In Fig. 1b all the diffraction peaks of the hollow spheres can be readily indexed to the cubic Y_2O_3 phase (JCPDS No. 83-0927), revealing that the $Y(OH)CO_3$:Eu^{3+} phosphor has successfully converted to Y_2O_3:Eu^{3+} on the SiO_2 mesoporous shell.

The functional groups on the as-synthesized MF (a), MF@SiO_2 (b), MF@SiO_2@$Y(OH)CO_3$:Eu^{3+} precursor (c), hollow SiO_2@Y_2O_3:Eu^{3+} microspheres annealed at 800 °C (d) were examined by the FT-IR spectra, as shown in Fig. 2. In the FT-IR spectrum for MF (Fig. 2a), the characteristic absorption bands at about 3376, 1577 (1493, 1348), 1162, 1009 and 814 cm^{-1} can be assigned to the respective vibrations of hydroxyl/amino (–OH/–NH_2), amino (–NH_2), amine (C–N), ether (C–O–C), and C–N–C

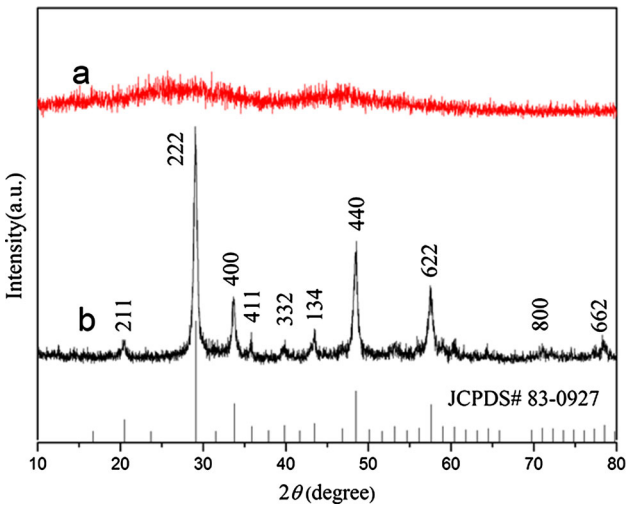

Fig. 1 XRD patterns of as-prepared precursor MF@SiO_2@-$Y(OH)CO_3$:Eu^{3+} (*a*) and SiO_2@Y_2O_3:Eu^{3+} calcined at 800 °C (*b*). The *vertical bars* show the peak positions and intensities for pure Y_2O_3 (JCPDS 83-0927) as a reference

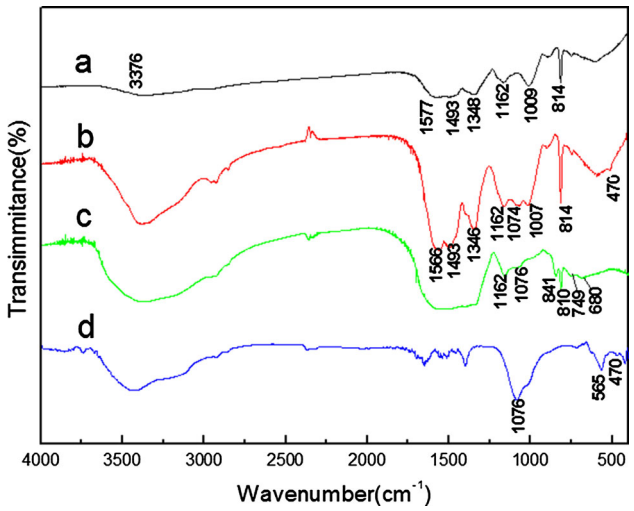

Fig. 2 FT-IR spectra of the as-obtained MF (*a*), MF@SiO_2 (*b*), MF@SiO_2@$Y(OH)CO_3$:Eu^{3+} precursor (*c*), SiO_2@Y_2O_3:Eu^{3+} hollow mesoporous microspheres annealed at 800 °C (*d*)

groups, suggesting the composition of MF [25, 26, 36–38].The peak at 814 cm^{-1} appeared in the curves a, b and c can be attributed to the core MF, illustrated the microspheres MF still exist before calcination. The FT-IR spectrum of Fig. 2b shows that in the MF@mSiO_2 sample, the peaks at 1074 and 470 cm^{-1} are due to the asymmetric stretch and bend vibrations of Si–O–Si in the mSiO_2 phase [32, 39]. After coated with a layer of SiO_2, the peak at around 1074 cm^{-1} in curves b, c and d can be attributed to the Si–O–Si asymmetric bond stretching vibration. Figure 2c shows the FT-IR spectrum of the precursor of MF@SiO_2@$Y(OH)CO_3$:Eu^{3+} without annealing. Besides the peaks in Fig. 2b, The peaks at 841, 749, and 680 cm^{-1} correspond to the deformation vibrations of CO, OH, and CO, respectively. The results indicate that the composition of the precursor is MF@mSiO_2@(Y,Eu)$(OH)CO_3$:Eu^{3+}. The FT-IR spectrum of hollow SiO_2@Y_2O_3:Eu^{3+} (Fig. 2d) shows that almost all of the functional groups related with MF disappear except for the peaks assigned to Si–O–Si (1076 cm^{-1}) and Si–O (470 cm^{-1}). Furthermore, a new band at 565 cm^{-1} can be assigned to the Y(Eu)–O stretching adsorption, which also confirms the formation of SiO_2@Y_2O_3:Eu^{3+} hollow spheres via the annealing process.

The structure of the samples was further investigated by SEM and TEM images in Fig. 3. Figure 3a, b show the SEM and TEM image of the bare MF microspheres. One can observe that the MF templates consist of highly uniform and well-dispersed microspheres with diameters of about 1.89 μm. It can also be seen that the surfaces of the monodisperse MF microspheres are very smooth. Figure 3c, d show the SEM and TEM images of the MF@SiO_2, meanwhile, the surfaces of the composite microspheres become rough due to the precipitation of a large amount of uniform SiO_2 nanoparticles. Naturally, the size of the core–shell-structured particles is about 2.1 μm larger than that of pure MF microspheres because the silica shell has been coated onto the core of MF microspheres during the in situ hydrolysis, condensation and coating process. Figure 3e, f show the image of the precursor MF@SiO_2@$Y(OH)CO_3$:Eu^{3+} before calcination. The uniform composite microspheres inherit the spherical morphology and the good dispersion of the MF@SiO_2 templates. Careful observation reveals that the thicknesses of the samples' shells increase slightly and much rougher in comparison with the composite templates, which mainly comes from the deposited precursors nanoparticles and the surfaces of precursor particles are much rougher than that of MF@SiO_2 due to the precipitation of a large amount of uniform $Y(OH)CO_3$:Eu^{3+} nanoparticles. Figure 3g and h exhibit the image of the spherical morphology of the SiO_2@Y_2O_3:Eu^{3+} sample after calcination at 800 °C. The contrast between the dark edge and the pale centre is direct evidence of the hollow nature of the microspheres and the diameter of hollow spheres is 2.2 μm. Compared with MF@SiO_2@$Y(OH)CO_3$:Eu^{3+} precursors microspheres, the hollow spheres show a little shrinkage caused by the core MF removed during calcination. One can clear resolution the porosity shell of hollow spheres were consist of large amount nanoparticles. As observed from high magnification (Fig. 3i, j) TEM images, a spherical particle contains tens of small sized nanoparticles (dark regions) that are separated by tens of pores (light regions) [40]. Moreover, the pores were randomly arranged but distributed throughout the whole particle. The size of the pores ranges from several nanometers to more than one hundred nanometers.

The thermal behavior of the as-prepared precursor was investigated by TGA–DTG measurements (Fig. 4). There are two major stages of sharp weight loss in the TGA curve at 396 and 520 °C, accompanying their corresponding exothermic peaks in the DTG curve (red line). The two rapid weight losses can be assigned to the dehydration and burning of the MF templates, respectively. In addition, a slight weight loss accompanied with a broad endothermic peak can be observed from 600 to 800 °C, which can be assigned to the conversion from the amorphous precursor to the crystalline Y_2O_3:Eu^{3+}. The residual weight percentage of the precursor is about 16 %, which accounts for the final SiO_2@Y_2O_3:Eu^{3+} product.

Figure 5 shows the N_2 adsorption–desorption isotherm and the corresponding pore size distributions of SiO_2@Y_2O_3:Eu^{3+} hollow mesoporous microspheres. The samples exhibit typical type-IV isotherms with H_3-typed hysteresis loops. From the pore distribution curve measured by the Barrett–Joyner–Halenda (BJH) method (insets), one can

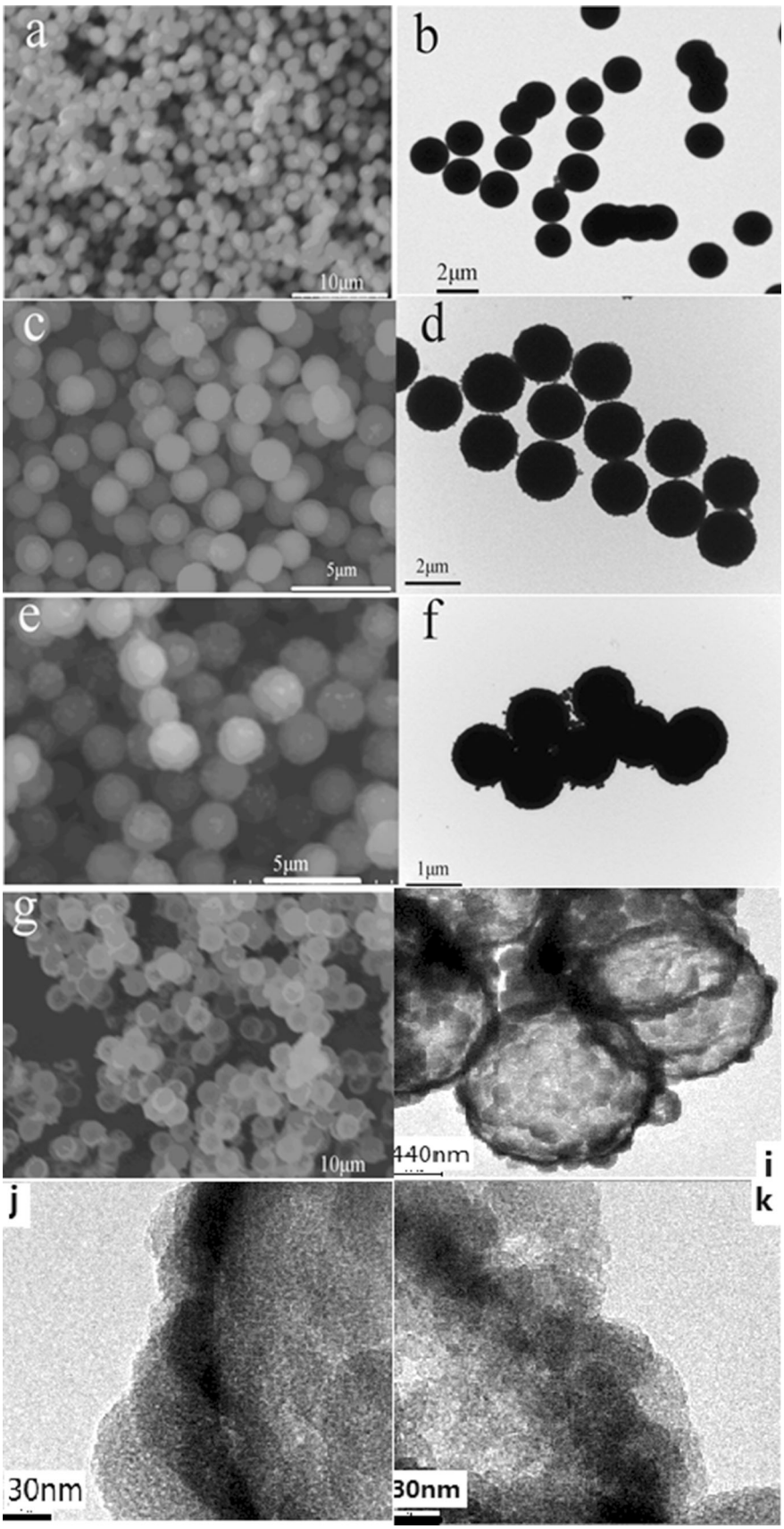

Fig. 3 SEM (*left*) and TEM (*right*) images of MF templates (**a**, **b**), MF@SiO_2 microspheres (**c**, **d**), MF@SiO_2@Y(OH)CO_3:Eu^{3+} precursor (**e**, **f**) and SiO_2@Y_2O_3:Eu^{3+} hollow mesoporous microspheres (**g**, **h**); the high (**j**, **k**) magnification TEM image of SiO_2@Y_2O_3:Eu^{3+} hollow mesoporous microspheres

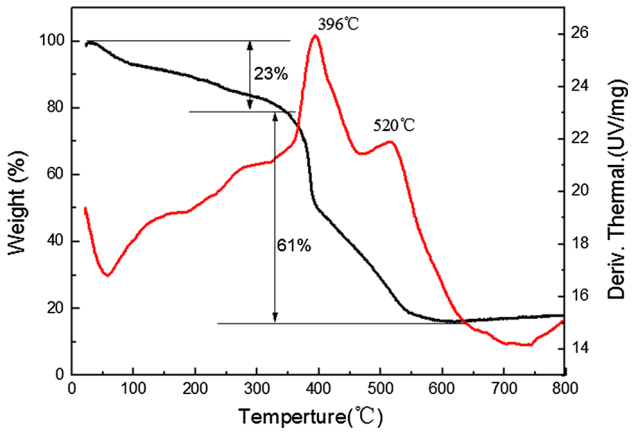

Fig. 4 TGA–DTG curves of MF@SiO_2@Y(OH)CO_3:Eu^{3+}

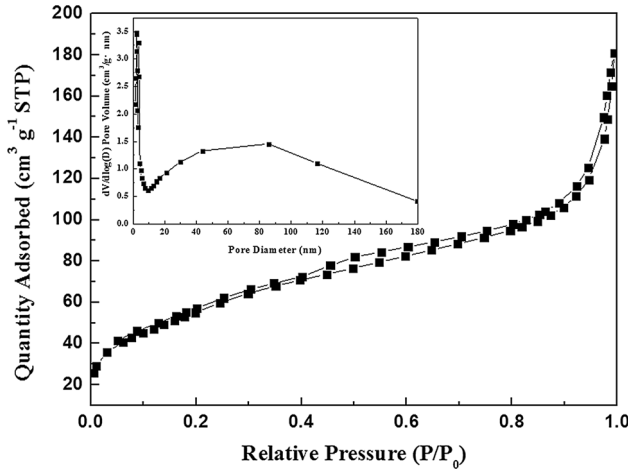

Fig. 5 Nitrogen adsorption–desorption isotherm and BJH desorption pore width distribution (*inset*) of SiO_2@Y_2O_3:Eu^{3+} hollow mesoporous spheres

see that the samples have obvious mesopores with a peak pore diameter of around 3 nm and decreased amount of macropores. The BET surface area and the total pore volume are 202.8 m^2/g and 0.28 cm^3/g, respectively. The unique structure of the spheres with pore walls and the hollow cavities may be ideal for molecule drug delivery.

The formation of SiO_2@Y_2O_3:Eu^{3+} hollow mesoporous microspheres is shown in Scheme 1. As shown in Scheme 1, Firstly, as-prepared MF microspheres used as templates. Subsequently, SiO_2 was coated onto the surface of the MF templates by a modified Stöber method, in the process of synthesizing, CTAB served as a structure-directing agent to form the mesoporous structure; Then, a simple homogeneous precipitation method was used to prepare the MF@mSiO_2@Y(OH)CO_3:Eu precursor; Finally, the hollow structured SiO_2@Y_2O_3:Eu^{3+} microspheres were obtained by annealing the precursor at 800 °C under an air atmosphere.

3.2 Photoluminescence properties

Figure 6 gives the excitation (left) and emission spectra (right) of SiO_2@Y_2O_3:Eu^{3+} (a), SiO_2@Y_2O_3:Eu^{3+}-IBU (b). As a whole, all the SiO_2@Y_2O_3:Eu^{3+} samples exhibit much similar PL spectra except for a little change in the intensity. It can be seen clearly that the excitation spectra consist of a broad band with a maximum at 254 nm due to the charge transfer band (CTB) between the O^{2-} and Eu^{3+} ions, and a series of weak transition lines with respect to the strong CTB of Eu^{3+}–O^{2-} in the range of 300–470 nm arising from f electrons of Eu^{3+}. In the emission spectra (right) upon excitation at 254 nm, the emission spectra were composed of a group of lines peaking at about 533, 579, 587, 592, 598, 610, 649, and 705 nm. They come from the $^5D_1$–$^7F_1$ and $^5D_0$–^7F_J (J = 0, 1, 2, 3, 4) transitions of the Eu^{3+} ions, respectively. The emission spectra is dominated by the red $^5D_0$–$^7F_2$ (610 nm) transition of the Eu^{3+} ions, which is an electric-dipole allowed transition and hypersensitive to the environment. Notably, the PL emission intensity of the drug loaded sample shows the stronger emission than that of unload sample, suggesting the potential to be tracked or detected during the drug release procedure.

3.3 Drug storage/delivery properties

Furthermore, the cumulative drug release from SiO_2@Y_2O_3:Eu^{3+} at pH 7 was detected. As shown in Fig. 7, the initial fast release could be attributed to IBU being weakly adsorbed onto the outer surface of the hollow SiO_2@Y_2O_3:Eu^{3+}, and the slow release of the remaining of IBU

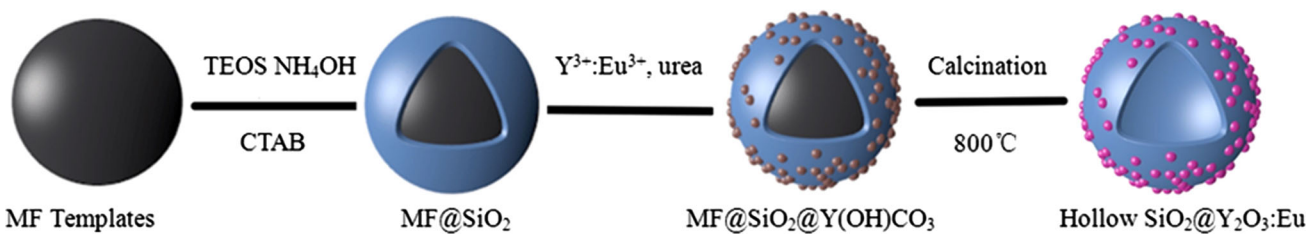

Scheme 1 Schematic illustration for the formation process of the hollow SiO_2@Y_2O_3:Eu^{3+} mesoporous microspheres

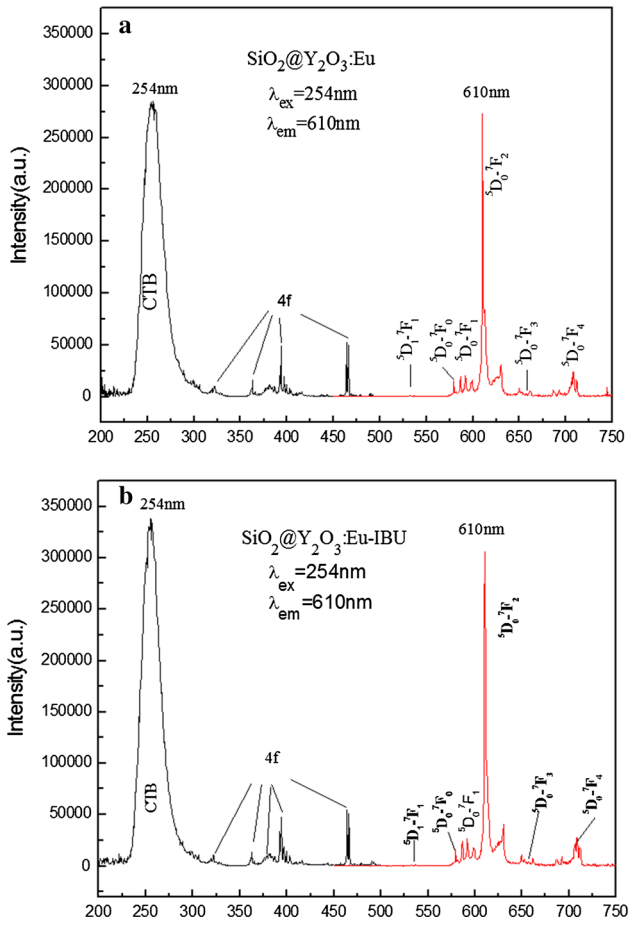

Fig. 6 The excitation (*left*) and emission (*right*) spectra of SiO_2@Y_2O_3:Eu^{3+} (**a**), SiO_2@Y_2O_3:Eu^{3+}-IBU (**b**) (Color figure online)

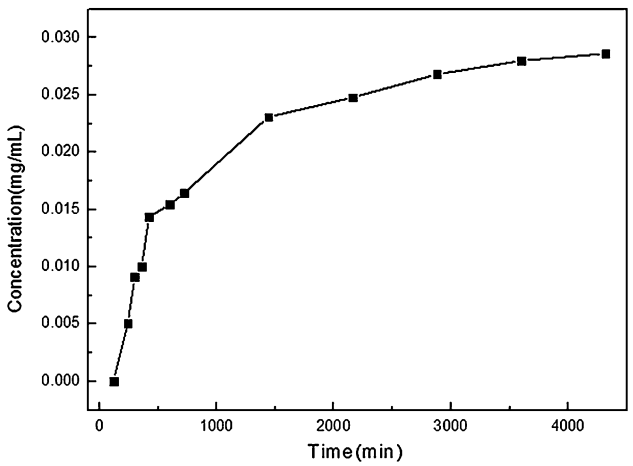

Fig. 7 Cumulative IBU release from SiO_2@Y_2O_3:Eu^{3+}-IBU at PBS

could be due to the strong interaction between IBU molecules and the internal surface of the hollow SiO_2@Y_2O_3:Eu^{3+}, which could be due to the numerous small pores in the SiO_2 shell with a stronger adsorption to IBU, and the drug release was almost completed after more than 50 h [41]. The loading content and entrapment efficiency for this system were calculated to be 4.2 and 14.4 %, respectively, using the corresponding equations.

$$\mathrm{LC}\% = \frac{\text{amount of IBU in composite spheres}}{\text{amount of IBU-loaded in composite spheres}} \times 100\%$$

$$\mathrm{EE}\% = \frac{\text{amount of IBU in compsite spheres}}{\text{total amount of IBU for drug loading}} \times 100\%$$

4 Conclusion

In summary, a hard-templating procedure has been demonstrated to prepare SiO_2@Y_2O_3:Eu^{3+} hollow mesoporous microspheres. This kind of composite microsphere combines the advantages of hollow, mesoporous structure and luminescence, which are employed as drug carriers to study the loading and release efficiency using IBU as a model drug. This functional drug carrier exhibits obvious sustained properties. More importantly, the proposed strategy to obtain the functional hollow inorganic composites provides a feasible and efficient approach to fabricating other hollow structures to satisfy the needs of various applications.

Acknowledgments The authors thank the ShanXi Provincial Science and Technology Foundation of China (20110321037-02), the ShanXi Provincial Natural Science Foundation of China (2015011016), ShanXi Provincial International Technological Cooperation of China (2012081020), and Taiyuan (110240) Bureau Science and Technology Research Projects Foundation of China for the financial support.

References

1. R.C. Lv, S.L. Gai, Y.L. Dai, F. He, N. Niu, P.P. Yang, Inorg. Chem. **53**(2), 998 (2014)
2. Y.F. Jiao, J. Guo, S. Shen, B.S. Chang, Y.H. Zhang, X.G. Jiang, W.L. Yang, J. Mater. Chem. **22**, 17636 (2012)
3. G. Wang, Q, Peng, Y. Li. Acc. Chem. Res. **44**, 322 (2011)
4. L.J. De Cock, S. De Koker, B.G. De Geest, J. Grooten, C. Vervaet, J.P. Remon, G.B. Sukhorukov, M.N. Antipina, Angew. Chem. Int. Ed. **49**, 6954 (2010)
5. W.R. Zhao, H.R. Chen, Y.S. Li, L. Li, M.D. Lang, J.L. Shi, Adv. Funct. Mater. **18**, 2780 (2008)
6. Z. Feng, Y. Li, D. Niu, L. Li, W. Zhao, H. Chen, L. Li, J. Gao, M. Ruan, J. Shi. Chem. Commun. **28**, 2629 (2008)
7. G.X. Yang, S.L. Gai, F.Y. Qu, P.P. Yang, ACS. Appl. Mater. Interfaces **5**, 5788 (2013)
8. N.M. Selivanova, A.E. Vandyukov, A.T. Gubaidullin, Y.G. Galyametdinov, Mater. Chem. Phys. **148**, 110 (2014)
9. B.A. Miura, N.H. Ferreira, P.F. Oliveira, E.H. de Faria, D.C. Tavares, L.A. Rocha, K.J. Ciuffi, E.J. Nassar, J. Lumin. **159**, 93 (2015)
10. L.Z. Tong, X.Z. Ren, X.D. Chen, H. Ding, X.W. Yang, H. Yang, Dyes Pigments **106**, 182 (2014)

11. E. Bernardo, G. Parcianello, S. Pilati, P. Colomboa, A.C.A. Delsing, H.T. Hintzen, J. Asian Ceram. Soc. **2**, 158 (2014)
12. W.T. Chen, H.S. Sheu, R.S. Liu, J.P. Attfield, J. Am. Chem. Soc. **134**, 8022 (2012)
13. T. Zhang, X. Zhu, C.C.W. Cheng, W.M. Kwok, H.L. Tam, J. Hao, D.W.J. Kwong, W.K. Wong, K.L. Wong, J. Am. Chem. Soc. **133**, 20120 (2011)
14. T.C. Liu, H. Kominami, H.F. Greer, W. Zhou, Y. Nakanishi, R.S. Liu, Chem. Mater. **24**, 3486 (2012)
15. P. Yang, Z.W. Quan, C.X. Li, H.Z. Lian, S.S. Huang, J. Lin, Microporous Mesoporous Mater. **116**, 524 (2008)
16. P. Yang, Z. Quan, Z. Hou, C. Li, X. Kang, Z. Cheng, J. Lin, Biomaterials **30**, 4786 (2009)
17. S. Gai, P. Yang, C. Li, W. Wang, Y. Dai, N. Niu, J. Lin. Adv. Funct. Mater. **20**, 1166 (2010)
18. Y.S. Li, J.L. Shi, Z.L. Hua, H.R. Chen, M.L. Ruan, Nano Lett. **3**, 609 (2003)
19. A.M. Collins, C. Spickermann, S. Mann, J. Mater. Chem. **13**, 1112 (2003)
20. Q. Peng, Y.J. Dong, Y.D. Li, Angew. Chem. Int. Ed. **42**, 3027 (2003)
21. A. Wolosiuk, O. Armagan, P.V. Braun, J. Am. Chem. Soc. **127**, 16356 (2005)
22. L. Z.Wang, Y. Ebina, K. Takada, T. Sasaki. Chem. Commun. 1074(2004)
23. Y.D. Xia, R. Mokaya, J. Mater. Chem. **15**, 3126 (2005)
24. P. Jiang, J.F. Bertone, V.L. Colvin, Science **291**, 453 (2001)
25. W.S. Choi, H.Y. Koo, D.Y. Kim, Langmuir **24**, 4633 (2008)
26. B. Friedel, S. Greulich-Weber, Small **2**, 859 (2006)
27. W.S. Choi, H.Y. Koo, W.T.S. Huck, J. Mater. Chem. **17**, 4943 (2007)
28. G. Jia, H.P. You, Y.H. Zheng, K. Liu, N. Guo, H.J. Zhang, CrystEngComm **12**, 2943 (2010)
29. Y.H. Han, S.L. Gai, P.A. Ma, L.Z. Wang, M.L. Zhang, S.H. Huang, P.P. Yang, Inorg. Chem. **52**, 9184 (2013)
30. Y.H. Fu, H.F. Jiu, L.X. Zhang, Y.X. Sun, Y.Z. Wang, Mater. Lett. **91**, 265 (2013)
31. I. Cho, J.G. Kang, Y.K. Sohn, Bull. Korean Chem. Soc. **35**, 575 (2014)
32. H. Liu, H.L. Li, Z.L. Ding, A.P. Fu, H.Y. Wang, P.Z. Guo, J.Q. Yu, C.G. Wang, X.S. Zhao, J. Clust. Sci. **23**, 273 (2012)
33. J. Zhang, Y.H. Wang, Z.G. Xu, H.X. Zhang, P.Y. Dong, L.N. Guo, F.H. Li, S.Y. Xin, W. Zeng, J. Mater. Chem. B **1**, 330 (2013)
34. G. Jia, H.P. You, Y.H. Song, Y.J. Huang, M. Yang, Zhang H. J. Inorg. Chem. **49**, 7721 (2010)
35. G. Jia, M. Yang, Y.H. Song, H.P. You, H.J. Zhang, Cryst. Growth Des. **9**, 301 (2009)
36. Y. Wu, Y. Li, L. Qin, J. Mater. Chem. B **1**(2), 204 (2013)
37. G. Jia, K. Liu, Y.H. Zheng, Y.H. Song, H.P. You, Cryst. Growth Des. **9**, 3702 (2009)
38. C.Y. Gao, S. Moya, H. Lichtenfeld, A. Casoli, H. Fiedler, E. Donath, H. Mohwald, Macromol. Mater. Eng. **286**, 355 (2001)
39. X. Ren, L. Tong, X. Chen, Phys. Chem. Chem. Phys. **16**(22), 10539 (2014)
40. W.H. Di, X.G. Ren, L.G. Zhang, C.X. Liu, S.Z. Lu, CrystEngComm **13**, 4831 (2011)
41. Z. Xu, D. Wang, M. Guan, ACS Appl. Mater. Int. **4**(7), 3424 (2012)